The Canadian Journal of Statistics

Vol. xx, No. yy, 2020, Pages 1–25

La revue canadienne de statistique

Modelling fine-scale correlation structures using hidden Markov models

BlindedA[1]* and BlindedB[2]

[1]*Author affiliations will go here in the accepted manuscript, but do NOT include them in your initial submission because it must be anonymous.*

[2]*Second Affiliation*

Key words and phrases: Association parameters; clustered data; mean parameters; missing data; pairwise likelihood; repeated measurements.

MSC 2010: Primary 62???; secondary 62???

Abstract:

Recent advances in high-frequency tagging technology have made a vast amount of movement data available in a variety of fields. This data can exhibit simultaneous behavioural processes occurring at different time scales, resulting in increasingly complicated dependence structures. These processes can be modelled through a hierarchical hidden Markov model (HHMM), which models the system as a nested structure of hidden Markov models (HMMs). At very short time scales, however, many basic assumptions of traditional HMMs are violated. We demonstrate how to incorporate fine-scale processes into the larger structure of HHMMs while maintaining computational efficiency. We apply our method to dive and accelerometer data collected from a northern resident killer whale off the coast of British Columbia, Canada.

Résumé: Insérer votre résumé ici. We will supply a French abstract for those authors who can't prepare it themselves. *La revue canadienne de statistique* xx: 1–25; 2020

1. INTRODUCTION

The field of animal movement is in the midst of a "data renaissance" where advancements in tagging technology have given rise to an explosion of data available for statistical modeling. In particular, some tagging technologies are capable of recording observations at rates of tens of hertz, resulting in time series containing millions of observations over the course of several hours. In response, researchers have introduced a variety of new statistical techniques to infer animal behavior from movement data (Hooten et al., 2017).

One of the most prevalent techniques in recent literature is the hidden Markov model (HMM), where observations depend upon the state of an associated unobserved behavioral process following Markovian dynamics (Patterson et al., 2017). Importantly, under the traditional HMM model, subsequent observations are assumed to be independent from one another after conditioning on the underlying behavioral process. However, this assumption is often violated in real world processes, especially when observations are taken at high frequencies. For example, the location of an animal at a given time is highly correlated with the location of that animal one second later. Several publications have dealt with this issue in the past, including the hidden movement Markov model (HMMM)

(Whoriskey et al., 2016) and the conditionally auto-regressive hidden Markov model (CarHMM) (Lawler et al., 2019). The CarHMM in particular explicitly models auto-correlation into an HMM while maintaining the structure needed to run the forward algorithm. It also only adds one additional parameter per possible hidden state.

Another issue that arises in high-frequency data is that several simultaneous behavioral processes may occur at different time scales. In this work, we consider an example where killer whales exhibit a variety of different types of dives at a coarse scale, but also exhibit many different types of swimming behaviors within dives at a fine scale. One solution to this issue is to use a hierarchical hidden Markov model (HHMM) (Leos Barajas et al., 2017; Adam et al., 2019). HHMMs model the entire time series in question as a nested structure of hidden Markov models (HMM) where each HMM corresponds to one behavioral process.

HMMs assume Markovian dynamics in the underlying process (i.e. that any observation Y_t depends only on the behavioral state X_t and Y_{t-1} when conditioned on all previous time steps). At the shortest time scales, however, observations often exhibit complicated dependence structures which cannot be easily captured by traditional HMMs, CarHMMs, or HHMMs. Examples included periodic fluking behavior in killer whales off the coast of Vancouver, BC, and swimming patterns of horn sharks of the coast of Southern California (Adam et al., 2019). With improvements in tagging technology allowing for data to be collected at very high frequencies, noisy and non-Markovian fine-scale processes are likely to persist.

One solution is to model the fine-scale behavior using a continuous-time model, which involves modelling the dynamics of an animal as the solution of a stochastic differential equation. Continuous-time models are more flexible than their discrete-time counterparts and can incorporate observations taken at irregular time intervals. Unfortunately, they are often computationally intractable and require approximate inference techniques such as Markov-chain Monte Carlo (MCMC) methods to fit.

For periodic behavior in particular, one way to avoid the use of continuous time models is to use signal processing techniques such as the Fourier transform on the raw data. The advantages of using Fourier analysis within an HMM has been recently demonstrated in the context of describing daily behavioral cycles of marine mammals (Heerah et al., 2017). In addition, Fourier analysis has previously been used in the field of animal movement to explain animal behavior (Fehlmann et al., 2017) and specifically fluking (Shorter et al., 2017) from accelerometer data. Thus, incorporating Fourier analysis of accelerometer data within the structure of an HMM appeared a promising simple approach to account for additional correlation in data that is cyclical in nature.

This work investigates how to incorporate fine-scale processes into the larger structure of hierarchical hidden Markov models while maintaining computational efficiency. We describe a general procedure that can be used to extract features from highly structured fine-scale behaviors that otherwise could not be modeled with existing HMM models. In addition, we bridge the gap between the discrete CarHMM and certain continuous-time stochastic process models by showing that the two are equivalent under certain conditions. We then perform a simulation study to compare the performance each existing model with ours in a controlled setting. Finally, we apply our method to dive data of a killer whale (*Orcinus orca*) from the threatened Northern resident population off the coast of British Columbia, Canada.

2. MODELS AND PARAMETER ESTIMATION

Traditional hidden Markov models (HMMs) are useful tools to *blah blah blah - quick (5-7words) restatement of the main advantage of HMM*, and will be used as the core structure of our models. However, traditional HMMs assume conditional independence between observations given the state sequence, and thus do not hold when the observations exhibit certain forms of significant correlation in time. Traditional HMMs model process autocorrelation with a single Markov chain, however many processes have temporal dependencies acting at different scales. *blah blah blah -quick restatements (5-15 words to potentially many sentences) of the main issues you are going to fix made a quick try at it, work on smoothing things. You can use some of the text I removed from below*. To account for each of these common additional dependence structures, we will explore three variations on the traditional HMM: the conditionally auto-regressive hidden Markov model (CarHMM), hierarchical hidden Markov model (HHMM), and HMM-DFT. We will show how each of these variations can be altered and combined to form a wide variety of new models.

2.1. The base structure of HMMs

An HMM is comprised of a sequence of unobserved states X_t, $t = 1, \ldots, T$, and an associated sequence of possibly high-dimensional observations Y_t, $t = 1, \ldots, T$. The Y_t's are often referred to as "emissions" and the index t typically refers to time. The X_t's form a Markov chain and take possible values $1, \ldots, N$. Their distribution is governed by the distribution of the initial state X_1 and the $N \times N$ transition probability matrix Γ, where $\Gamma_{ij} = \Pr(X_{t+1} = j | X_t = i)$, for $t = 1, \ldots, T-1$, and $i, j = 1, \ldots, N$. We assume that X_1 follows the chain's stationary distribution, which is denoted by $\delta \in \mathbb{R}^N$, with i^{th} component $\delta_i = \Pr\{X_1 = i\},\ i = 1, \ldots, N$. A Markov chain's stationary distribution is determined by its probability transition matrix via $\delta = \delta\Gamma$ and $\sum_{i=1}^{N} \delta_i = 1$. The distribution of an emission Y_t depends only on the corresponding state X_t and no other observations or hidden states: $p\left(y_t | \{X_1, \ldots, X_T\}, \{Y_1, \ldots, Y_T\} / \{Y_t\}\right) = p(y_t | X_t)$. These conditional distributions are governed by state-dependent parameters. If $X_t = i$, then the state-dependent parameter is $\theta^{(i)}$ and we denote the conditional distribution of Y_t given $X_t = i$ by its conditional density or probability mass function, denoted $f^{(i)}(\cdot; \theta^{(i)})$, or sometimes $f^{(i)}(\cdot)$. Figure 1a represents the dependence structure of an HMM.

Using observed emissions, here denoted $y = (y_1, \ldots, y_T)$, we can find the maximum likelihood estimates of the parameters Γ and $\Theta \equiv (\theta^{(1)}, \ldots, \theta^{(N)})$. We write the likelihood $\mathcal{L}_{\text{HMM}}$ using the well-known *forward algorithm* (Zucchini et al., 2016):

$$\mathcal{L}_{\text{HMM}}(y; \Theta, \Gamma) = \delta P(y_1; \Theta) \prod_{t=2}^{T} \Gamma P(y_t; \Theta) \mathbf{1}_N$$

where $\mathbf{1}_N$ is an N-dimensional column vector of ones and $P(y_t; \Theta)$ is an $N \times N$ diagonal matrix with $(i, i)^{th}$ entry $f^{(i)}(y_t; \theta^{(i)})$.

Following Leos Barajas et al. (2017), we parameterize the $N \times N$ transition probability matrix Γ in a way that forces the entries of the matrix to be non-negative and for the rows to sum to 1:

$$\Gamma_{ij} = \frac{\exp(\eta_{ij})}{\sum_{k=1}^{N} \exp(\eta_{ik})},$$

where $\eta \in \mathbb{R}^{N \times N}$ and η_{ii} is set to zero for identifiability. Then $\mathcal{L}_{\text{HMM}}(y; \Theta, \Gamma)$ can be maximized using a wide range of optimizer. For simplicity, we will continue to use Γ in our notation, suppressing the reparameterization in terms of η.

2.2. Relaxing the conditional independence assumption with a CarHMM

The CarHMM, introduced by Lawer et al. (2019), explicitly models auto-correlation in observation within an HMM. Like a traditional HMM, a CarHMM is made up of a Markov chain of unobserved states $X_1, \ldots, X_T$ that can take on values $1, \ldots, N$, with transition probability matrix Γ and initial distribution δ

equal to the stationary distribution of Γ. Unlike a traditional HMM, the CarHMM assumes that the distribution of Y_t conditioned on $X_1, \ldots, X_T$ and $Y_1, \ldots, Y_{t-1}$, depends on *both* X_t *and* Y_{t-1} rather than only X_t. The first emission Y_1 is assumed to be fixed as an initial value which does not depend upon X_1. Figure 1b shows the dependence structure of a CarHMM.

We denote the conditional distribution of Y_t given $Y_{t-1} = y_{t-1}$ and $X_t = i$ as $f^{(i)}(\cdot|y_{t-1}; \theta^{(i)})$ or simply $f^{(i)}(\cdot|y_{t-1})$. For example, one could assume that this conditional distribution is Normal with parameters $\theta^{(i)} = \{\mu^{(i)}, \sigma^{(i)}, \phi^{(i)}\}$ where:

$$\mathbb{E}(Y_t|Y_{t-1} = y_{t-1}, X_t = i) = \phi^{(i)}\, y_{t-1} \;+\; (1 - \phi^{(i)})\, \mu^{(i)}$$

and

$$\mathbb{V}(Y_t|Y_{t-1} = y_{t-1}, X_t = i) = (\sigma^{(i)})^2.$$

The likelihood for the CarHMM can be easily calculated using the forward algorithm. As previously, let y be the vector of observed emissions. Then

$$\mathcal{L}_{\text{CarHMM}}(y; \Theta, \Gamma) = \delta \prod_{t=2}^{T} \Gamma P(y_t|y_{t-1}; \Theta) \mathbf{1}_N \tag{1}$$

where $P(y_t|y_{t-1}; \Theta)$ is an $N \times N$ diagonal matrix with $(i,i)^{th}$ entry equal to $f^{(i)}(y_t|y_{t-1}; \theta^{(i)})$.

While CarHMMs can model auto-correlation within the observation sequence, they fail when observations are taken at irregular time intervals. Another way to model a stochastic process is to use a stochastic differential equation

(SDE). As an example, Michelot & Blackwell (2019) model the movement of an animal as the solution to the following stochastic differential equation, which they refer to as a state-switching Ornstein-Uhlenbeck process:

$$dY_t = \beta^{(X_t)}(\gamma^{(X_t)} - Y_t)dt + \omega^{(X_t)}dW_t \tag{2}$$

where X_t is some stochastic process which defines the hidden behaviour of the animal at time t, $\beta^{(X_t)}$ relates to rate at which the process returns to its mean value, $\gamma^{(X_t)}$ is the long-term mean value of the process, $\omega^{(X_t)}$ is related to short-term variance, and W is a Wiener process. Unlike HMMs, $t \in \mathbb{R}$ indexes a continuous time process and is therefore not necessarily an integer. If the behavioral state X_t is known and does not change between observations, the solution to Equation (2) is known to be the following (Michelot and Blackwell, 2019):

$$Y_{t+\Delta t}|X_t \sim \mathcal{N}\left((1-e^{-\beta^{(X_t)}\Delta t})\gamma^{(X_t)} + e^{-\beta^{(X_t)}\Delta t}Y_t, \quad \frac{\omega^{(X_t)^2}}{2\beta^{(X_t)}}(1-e^{-2\beta^{(X_t)}\Delta t})\right) \tag{3}$$

where Δt is the time difference between any two observations Y_t and $Y_{t+\Delta t}$. Most continuous time models are difficult to incorporate into an HHMM and require MCMC methods to fit. However, under certain conditions, the CarHMM is equivalent to a state-switching Ornstein-Uhlenbeck process. This gives new interpretation to the learned parameters of the CarHMM in the context of a continuous-time model.

Theorem 1. *If the following conditions are met:*

1. *The hidden behavioural process X from Equation 2 follows a Markov chain with N possible states and transitions occur at equi-spaced time stamps $(\Delta t, \ldots, (T-1)\Delta t)$,*
2. *Observations of the SDE from Equation 2 are taken at times $(0, \Delta t, \ldots, (T-1)\Delta t)$,*

then the observations Y are equivalent to the output of a conditionally auto-regressive hidden Markov model with normal emission distributions and parameters $\Theta = (\theta^{(1)}, \ldots, \theta^{(N)})$; $\theta^{(i)} = \{\mu^{(i)}, \sigma^{(i)}, \phi^{(i)}\}$, where:

$$\mu^{(i)} = \gamma^{(i)}, \qquad \sigma^{(i)} = \sqrt{\frac{\omega^{(i)2}}{2\beta^{(i)}}(1 - e^{-2\beta^{(i)}\Delta t})}, \qquad \phi^{(i)} = e^{-\beta^{(i)}\Delta t} \tag{4}$$

See the appendix for a proof of Theorem 1.

2.3. Incorporating different scales of correlations with HHMM

HHMM accounts for different levels of correlation by modeling a coarse-scale process and a fine-scale process, each of which with an HMM *CITATION(s)*. The coarse-scale process is an HMM as defined previously, where $X_1, \ldots, X_T$ make up an unobserved Markov chain with N possible states and $Y_1, \ldots, Y_T$ are the corresponding observed responses. In the hierarchical setting, each state X_t emits yet another sequence of fine-scale unobserved states, $X_t^* \equiv (X_{t,1}^*, \ldots, X_{t,T_t^*})$ and a sequence of fine-scale observed emissions, $Y_t^* \equiv (Y_{t,1}^*, \ldots, Y_{t,T_t^*})$. The fine-scale process (X_t^*, Y_t^*) makes up another HMM with parameters that depend on the value of X_t. Specifically, if $X_t = i$, then the distribution of X_t^* is characterized by an $N_t^* \times N_t^*$ transition probability matrix $\Gamma^{*(i)}$ and initial distribution $\delta^{*(i)}$, which we assume is equal to the stationary distribution of the chain. For simplicity, we take $N_t^* \equiv N^*$ although this is not necessary.

The distribution of Y_{t,t^*} given $X_{t,t^*} = i^*$ and $X_t = i$ is governed by a parameter $\theta^{(i,i^*)}$ and has density or probability mass function denoted $f^{*(i,i^*)}\left(\cdot;\theta^{(i,i^*)}\right)$ or simply $f^{*(i,i^*)}(\cdot)$.We denote the fine-scale emission parameter vector corresponding to $X_t = i$ with $\Theta^{*(i)} = \left(\theta^{(i,1)},\ldots,\theta^{(i,N^*)}\right)$.

Given the coarse-scale states, $X_1,\ldots,X_T$, the T fine-scale processes $(X_1^*,Y_1^*),\ldots,(X_T^*,Y_T^*)$, are independent HMMs. Depending upon the process being modeled, it is possible to force certain parameters to be shared across different coarse or fine states. For example, in the killer whale case study (Section 4), we force the fine-scale emission parameters to be shared across coarse-scale hidden states (i.e. $\theta^{(1,i^*)} = \ldots = \theta^{(N,i^*)}$ for $i^* = 1,\ldots,N^*$). Figure 1c represents the dependence structure for an HHMM.

Due to the nested structure of the hierarchical hidden Markov model, the likelihood is easy to calculate via the forward algorithm. Let y be the T-vector of the observed coarse-scale emissions and y^* be the $(T_1^* + \cdots + T_T^*)$-vector of the observed fine-scale emissions. Let $\Theta^* \equiv \{\Theta^{*(1)},\ldots,\Theta^{*(N)}\}$ denote the collection of all fine-scale emission parameters and let $\Gamma^* \equiv \{\Gamma^{*(1)},\ldots,\Gamma^{*(N)}\}$ denote the collection of all fine-scale transition probability matrices. The likelihood of the observed data is then

$$\mathcal{L}_{\text{HHMM}}(y, y^*; \Theta, \Theta^*, \Gamma, \Gamma^*) = \delta P(y_1, y_1^*; \Theta, \Theta^*, \Gamma^*) \prod_{t=2}^{T} \Gamma P(y_t, y_t^*; \Theta, \Theta^*, \Gamma^*) \mathbf{1}_N$$

where $P(y_t, y_t^*; \Theta, \Theta^*, \Gamma^*)$ is an $N \times N$ diagonal matrix with iith entry corresponding to $X_t = i$ and equal to $f^{(i)}(y_t)\mathcal{L}_{\text{HMM}}\left(y_t^*; \Theta^{*(i)}, \Gamma^{*(i)}\right)$.

For more information on specific considerations for HHMMs, such as incorporating covariates into the probability transition matrix, state decoding, model selection and model checking, see Adam et al. (2019).

2.4. The HMM with discrete Fourier transform (HMM-DFT)

The HMM with discrete Fourier transform, or HMM-DFT, incorporates hierarchical structure into an HMM differently than an HHMM. In particular, the fine-scale process is no longer modeled with an HMM and instead summarized using its Fourier transform. For simplicity, we assume that the length of the fine-scale processes is constant (i.e. that $T_t^* = T^*$), although this need not be the case in general. Suppose that the fine-scale process y_t^* does not switch hidden states, but does exhibit significant periodic behaviour. We then suggest using the discrete Fourier transform (DFT) on y_t^*:

$$DFT\{y_t^*\}(k) := \hat{y}_t^{*(k)} = \sum_{t^*=1}^{T^*} y_{t,t^*}^* \exp\left(-i\frac{2\pi k}{T^*}(t^* - 1)\right), \quad k = 0, 1, \ldots, T^* - 1.$$

Summary statistics can then drastically reduce the dimension of $\hat{y}_t^*$. One example is as follows:

$$z_t^{*(1)} := \mathcal{R}\left(\hat{y}_t^{(0)}\right) \qquad z_t^{*(2)} := \frac{1}{T^*}\sum_{k=1}^{\tilde{\omega}} |\hat{y}_t^{(k)}|^2 \tag{5}$$

In words, $z_t^{*(1)}$ is the average value of y_t^* and $z_t^{*(2)}$ is the squared 2-norm of the component of y_t^* that can be attributed to frequencies between 1 and $\tilde{\omega}$ periods per window length T^*. The maximum frequency $\tilde{\omega}$ is a problem-specific tuning parameter which should be selected with care. These summary statistics are just one possible choice to describe each window; other choices include the dominant frequency and amplitude of y_t^*. Figure 1d shows a graphical representation of the HMM-DFT.

Once z_t^* is calculated, it can be treated as an observation of the coarse-scale HMM and incorporated into the emission distribution $f^{(i)}\left(y_t, z_t^*; \theta^{(i)}\right)$, or more succinctly $f^{(i)}\left(y_t, z_t^*\right)$. In total, the likelihood of the hierarchical HMM-DFT is as follows:

$$\mathcal{L}_{\text{HMM-DFT}}(y, z^*; \Theta, \Gamma) = \delta P(y_1, z_1^*; \Theta) \prod_{t=2}^{T} \Gamma P(y_t, z_t^*; \Theta) \mathbf{1}_N \tag{6}$$

where $P(y_t, z_t^*; \Theta)$ is an $N \times N$ diagonal matrix with $(i,i)^{th}$ entry equal to $f^{(i)}\left(y_t, z_t^*; \theta^{(i)}\right)$.

It is possible to accommodate unequal time steps within y_t^* by using the non-uniform discrete Fourier transform (NDFT) (Bagchi and Mitra, 1999). We do not describe the method in detail here, but the generalization is straightforward.

2.5. General hierarchical structures

In addition to the models described above, the fine-scale process Y_t^* can be modeled using *any* parametric model which admits an easy-to-compute likelihood. The fine-scale likelihood $\mathcal{L}_{\text{HMM}}$ from the HHMM likelihood is then replaced by the likelihood of the general fine-scale model, $\mathcal{L}_{\text{fine}}(\mathbf{y}_t^*; \Theta^{*(i)})$:

$$\mathcal{L}_{\text{coarse}}(y, y^*; \Theta, \Theta^*, \Gamma) = \delta P(y_1, y_1^*; \Theta, \Theta^*) \prod_{t=2}^{T} \Gamma P(y_t, y_t^*; \Theta, \Theta^*) \mathbf{1}_N$$

where $P(y_t, y_t^*; \Theta, \Theta^*)$ is an $N \times N$ diagonal matrix with $(i,i)^{th}$ entry corresponding to $X_t = i$ and equal to $f^{(i)}\left(y_t; \Theta^{(i)}\right) \mathcal{L}_{\text{fine}}\left(y_t^*; \Theta^{*(i)}\right)$. This definition is straightforward to extend to the CarHMM as well:

$$\mathcal{L}_{\text{coarse}}(y, y^*; \Theta, \Theta^*, \Gamma) = \delta \prod_{t=2}^{T} \Gamma P(y_t, y_t^* | y_{t-1}; \Theta, \Theta^*) \mathbf{1}_N$$

where $P(y_t, y_t^* | y_{t-1}; \Theta, \Theta^*)$ is an $N \times N$ diagonal matrix with $(i,i)^{th}$ entry corresponding to $X_t = i$ and equal to $f^{(i)}\left(y_t | y_{t-1}; \Theta^{(i)}\right) \mathcal{L}_{\text{fine}}\left(y_t^*; \Theta^{*(i)}\right)$.

Possible candidates for the fine-scale model include any of the models described in the previous subsections (HMM, CarHMM, state-switching OU, HHMM, and HMM-DFT). These five models can act as initial building blocks in a practitioner's toolbox to construct increasingly complex hierarchical models based on HMMs. In the sections that follow, we perform both a simulation study and real-world case study modelling killer whale dive behaviour using models constructed from these building blocks.

3. SIMULATION STUDY

We base the following simulated study on the acceleration data of a killer whale's dive sequence. The parameters used to generate the data are loosely based on those learned from the case study in Section 4. We fit four separate models to the simulated data and compare their test the accuracy of each on a simulated test data set.

3.1. Data Simulation

500 separate sequences of 100 killer whale dives were simulated according to an HMM, where the hidden Markov chain X was a collection of dive types and the observations Y were the corresponding dive durations (in seconds). Each dive could be one of $N = 2$ dive types, and the duration of the t^{th} dive, Y_t, followed a gamma distribution whose parameters $\theta^{(i)}$ were dependent on the dive type $X_t = i$. We parameterize the gamma distribution by its mean and variance:

$$\Gamma = \begin{pmatrix} 0.5 \; 0.5 \\ \\ 0.5 \; 0.5 \end{pmatrix}, \qquad \delta = \begin{pmatrix} 0.5 \; 0.5 \end{pmatrix},$$

$$Y_t | X_t \sim \text{Gamma},$$

$$\mathbb{E}(Y_t|X_t = 1) = 15s, \qquad \mathbb{E}(Y_t|X_t = 2) = 60s,$$

$$\mathbb{V}(Y_t|X_t = 1) = 25s^2, \qquad \mathbb{V}(Y_t|X_t = 2) = 100s^2.$$

Once the dive durations were calculated for all 100 dives, dive t was broken into a sequence of $T_t^* = \lfloor Y_t/2 \rfloor$ two-second segments (the end of the dive sequence was discarded) which made up a second fine-scale hidden Markov model. Each two second segment was assigned one of $N^* = 2$ behaviours (active swimming or passive gliding) according to a fine-scale Markov chain $X_t^* \equiv \left(X_{t,1}^*, \ldots, X_{t,T_t^*}^*\right)$. The probability transition matrices for these fine-scale Markov chains were set as

$$\Gamma^{*(1)} = \begin{pmatrix} 0.5\,0.5 \\ \\ 0.9\,0.1 \end{pmatrix}, \qquad \Gamma^{*(2)} = \begin{pmatrix} 0.8\,0.2 \\ \\ 0.3\,0.7 \end{pmatrix},$$

where $\Gamma^{*(1)}$ was used for dives where $X_t = 1$ and $\Gamma^{*(2)}$ was used for dives where $X_t = 2$.

Each two-second sub-dive window had 100 associated acceleration readings, $Y_{t,t^*}^* \equiv \left(Y_{t,t^*,1}^*, \ldots, Y_{t,t^*,100}^*\right)$. To accurately recreate active swimming versus passive gliding on the fine-scale Markov chain, the DFT of each two-second segment $\hat{Y}_{t,t^*}^*$ was simulated such that $Z_{t,t^*}^{*(1)}$ and $Z_{t,t^*}^{*(2)}$ (see Eq. 5) have the following distributions:

$$\left(Z^{*(1)}_{t,t^*} | Z^{*(1)}_{t,t^*-1}, X^*_{t,t^*} = 1\right) \sim \mathcal{N}\left(\phi^{*(1)} Z^{*(1)}_{t,t^*-1} + (1 - \phi^{*(1)})\mu^{*(1)}, (\sigma^{*(1)})^2\right)$$

$$\left(Z^{*(1)}_{t,t^*} | Z^{*(1)}_{t,t^*-1}, X^*_{t,t^*} = 2\right) \sim \mathcal{N}\left(\phi^{*(2)} Z^{*(1)}_{t,t^*-1} + (1 - \phi^{*(2)})\mu^{*(2)}, (\sigma^{*(2)})^2\right)$$

$$\mu^{*(1)} = 0.0, \;\; \sigma^{*(1)} = 0.05, \;\; \phi^{*(1)} = 0.99$$

$$\mu^{*(2)} = 0.0, \;\; \sigma^{*(2)} = 0.1, \;\; \phi^{*(2)} = 0.95$$

$$\left(Z^{*(2)}_{t,t^*} | X^*_{t,t^*} = 1\right) \sim \text{Gamma}\left(\alpha^{*(1)}, \beta^{*(1)}\right)$$

$$\left(Z^{*(2)}_{t,t^*} | X^*_{t,t^*} = 2\right) \sim \text{Gamma}\left(\alpha^{*(2)}, \beta^{*(2)}\right)$$

$$\alpha^{*(1)} = 10.10, \quad \beta^{*(1)} = 1.00$$

$$\alpha^{*(2)} = 305.94, \quad \beta^{*(2)} = 1.00$$

Sub-dive behavior 1 corresponds to passive gliding while sub-dive behaviour 2 corresponds to active swimming with a dominant frequency of $\frac{1}{2}s^{-1}$. Sub-dive behaviors 1 and 2 are the same for both dive types. See the appendix for more details regarding procedure for simulating $\hat{Y}^*$ and Y^* such that Z^* has the preceding distribution. Figure 2 shows the first 5 dives of one simulated data set.

3.2. Model Formulation

The building blocks from the previous section were used to build a well-specified model for this simulated data. Specifically, we used a hierarchical HMM where the sequence of dive durations Y was modeled using a simple HMM, and the fine-scale process Z^* was modeled using a HMM-DFT with explicit autocorrelation in $Z^{*(1)}$. Naturally, we refer to this model as the **CarHHMM-DFT**. Figure 3 shows a graphical representation of this model.

On the coarse scale, the dive types follow a Markov chain with $N = 2$ possible states and unknown probability transition matrix Γ. The duration of a dive follows a gamma distribution which depends upon the dive type and unknown parameters $\Theta = \{\{\mu^{(1)}, \sigma^{(1)}\}, \{\mu^{(2)}, \sigma^{(2)}\}\}$.

On the fine scale, the sub-dive behavior of each two-second window comprises a Markov chain with $N^* = 2$ possible states and unknown probability transition matrices $\Gamma^{*(1)}$ and $\Gamma^{*(2)}$, depending upon the dive type. Each two-second window is summarized by the observations $Z^{*(1)}_{t,t^*}$ and $Z^{*(2)}_{t,t^*}$. The distribution of $Z^{*(1)}_{t,t^*}$ is Normal and its parameters depend upon the sub-dive behavior X^*_{t,t^*} and $Z^{*(1)}_{t,t^*-1}$. In particular:

$$\mathbb{E}(Z^{*(1)}_{t,t^*} | Z^{*(1)}_{t,t^*-1} = z, X^*_{t,t^*} = i) = \phi_1^{*(i)} z + (1 - \phi_1^{*(i)})\mu_1^{*(i)}$$

$$\mathbb{V}(Z^{*(1)}_{t,t^*} | Z^{*(1)}_{t,t^*-1} = z, X^*_{t,t^*} = i) = \left(\sigma_1^{*(i)}\right)^2.$$

The distribution of $Z^{*(2)}_{t,t^*}$ is gamma and its parameters depend upon only X^*_{t,t^*} (not X_t):

$$\mathbb{E}(Z^{*(2)}_{t,t^*} | Z^{*(1)}_{t,t^*-1} = z, X^*_{t,t^*} = i) = \mu_2^{*(i)}$$

$$\mathbb{V}(Z^{*(2)}_{t,t^*}|Z^{*(1)}_{t,t^*-1} = z, X^*_{t,t^*} = i) = \left(\sigma_2^{*(i)}\right)^2.$$

None of the fine-scale emission distributions depend upon dive type. In total the parameters to estimate are

$$\Gamma, \qquad \Gamma^* = \{\Gamma^{*(1)}, \Gamma^{*(2)}\} \qquad \text{(probability transition matrices)},$$

$$\Theta = \{\{\mu^{(1)}, \sigma^{(1)}\}, \{\mu^{(2)}, \sigma^{(2)}\}\} \qquad \text{(coarse-scale emission parameters), and}$$

$$\Theta^* = \{\Theta^{*(1)}, \Theta^{*(2)}\} \qquad \text{(fine-scale emission parameters), where}$$

$$\Theta^{*(i^*)} = \{\{\mu_1^{*(i^*)}, \sigma_1^{*(i^*)}, \phi_1^{*(i^*)}\}, \{\mu_2^{*(i^*)}, \sigma_2^{*(i^*)}\}\} \qquad (Z^{*(1)} \text{ and } Z^{*(2)} \text{ parameters}).$$

The likelihood of this model is still easy to calculate using the forward algorithm, and it can be maximized with respect to the parameters above. See the appendix for details of likelihood evaluation. Figure 3 shows the corresponding graphical model.

Including the CarHHMM-DFT described above, four different models were fit to the simulated data sets:

1. A **CarHHMM-DFT** as described above.
2. An **HHMM-DFT**, which is similar to the model above, but with no modeled auto-correlation, i.e. $\phi_1^{*(i^*)} = 0$ for $i^* = 1, 2$.
3. A **CarHHMM**, which is similar to the model above, but without $Z^{*(2)}$ as an observation (i.e $\Theta^{*(i^*)} = \{\mu_1^{(i^*)}, \sigma_1^{(i^*)}, \phi_1^{(i^*)}\}$, $i^* = 1, 2$).

4. A **CarHMM-DFT**, which is similar to the CarHHMM-DFT, but with $N = 1$ instead of $N = 2$ on the coarse scale. This is equivalent to loosing the coarse level of the hierarchical structure, as there is only one dive type.

Each of the last three models leaves out one important aspect of the full CarHHMM-DFT. The CarHMM-DFT lacks a hierarchical structure, the HHMM-DFT is missing auto-correlation within the fine-scale observations, and the CarHHMM does not have access to the Fourier transform sums $(Z^{*(2)})$ as observations.

3.3. Simulation Results

All models were run on the Cedar Compute Canada cluster with 1 CPU and 4 GB of dedicated memory per model. Each model was able to decode the fine-scale hidden states of the process almost perfectly except for the CarHHMM, whose accuracy was 89%. This is intuitively clear because the distribution of $Z^{*(2)}$ varies between fine-scale states much more than that of $Z^{*(1)}$. For the coarse-scale hidden states, the CarHMM-DFT lacked a hierarchical structure and could not make any predictions at all. The other three models all achieved an accuracy of approximately 90%, with the CarHHMM slightly more likely to categorize a dive as dive type 2 than the other models. Figure 4 shows the decoded state probabilities for both the fine- and coarse- scales. Table 1 lists the accuracy and training times of each model.

For the emission distributions of dive duration, Figure 5 shows the empirical joint density of $\hat{\mu}$ and $\hat{\sigma}$ for the CarHHMM-DFT. The supplementary material shows the empirical joint densities for all other models and features.

Estimates of standard error using the observed Fisher information tended to be underestimates due to correlation between $\hat{\mu}$ and $\hat{\sigma}$. In addition, $\hat{\sigma}$ tends to be an underestimate of σ for all models and dive types. This finding is consistent with properties of MLEs for standard deviation, especially with a small sample size. The CarHMM-DFT model in particular is not well specified one the coarse-scale and severely underestimates σ. A full table of parameter estimates for all models is shown in the supplementary material.

For acceleration ($Z^{*(1)}$), both the CarHMM-DFT and the CarHHMM-DFT regularly converged to the correct parameters with very little standard error. However, the estimated standard error based on the observed Fisher information regularly overestimated the empirical standard error of $\hat{\mu}$ for both of these models. The HHMM-DFT regularly overestimates the variance $Z^{*(1)}$ since it does not incorporate auto-correlation into the emission distribution of $Z^{*(1)}$. The CarHHMM has large biases in many of its parameter estimates, especially in sub-dive state 2. See the supplementary material for a detailed breakdown of parameter values for acceleration emission distributions.

For all models there is no bias in the parameter estimates for the distribution of the Fourier sums ($Z^{*(2)}$). One exception is the CarHHMM, which does not model $Z^{*(2)}$ as an observation at all. The standard error estimates based on the observed Fisher information closely approximate the empirical standard error. The supplementary material also shows a detailed breakdown of the emission distribution of $Z^{*(2)}$ for all models.

Estimates of the coarse-scale probability transition matrix Γ for all models (except for the CarHMM-DFT) are very accurate, with empirical standard errors of approximately 0.02 and biases of nearly zero. This is significantly less than the estimate of standard error based on the observed Fisher information, which is about 0.08 for all models. For the fine-scale transition matrices Γ^*, the HHMM-DFT and CarHHMM-DFT both showed practically no bias with standard errors on the order of 10^{-2}. One notable exception is the standard error of $\hat{\Gamma}^{*(1)}_{12}$, whose standard error was on the order of 10^{-4}, much lower than the observed Fisher information would predict. The CarHMM-DFT is mis-specified, so its results cannot be easily interpreted, but $\hat{\Gamma}^*$ regularly converged to a constant value with a standard error on the order of 10^{-2}. The CarHHMM consistently overestimated the trace of $\Gamma^{*(i^*)}$. Again, one notable exception is $\hat{\Gamma}^{*(1)}_{12}$, which had almost no bias and was remarkably consistent. See the supplementary material for a full list of estimates and standard errors.

4. KILLER WHALE CASE STUDY

The CarHHMM-DFT was used to analyze dive data from a Northern Resident Killer Whale (NRKW) off the coast of British Columbia, Canada. Acceleration data can be a good proxy for energy expenditure (Green et al., 2009), but studies suggest that the animal's behavioral state must be taken into account to obtain accurate estimates (Jeanniard du Dot et al., 2016). Therefore, understanding both the behavioral state of the killer whale as well as the distribution of accelerometer data within each behavioral state is import to understand the energetic requirements of killer whales. This knowledge can help ecologists understand the animal's energetic requirements and which in turn can help conservation efforts.

4.1. Data Collection and Preprocessing

The data used in this study was collected on September 2, 2019 from 12:49 pm to 6:06 pm and consists of depth and acceleration in three orthogonal directions. Observations were collected at a rate of 50 Hz. Tagging the killer whale caused anomalous behavior before 1:20 pm and after 6:00 pm, so observations in this time range were ignored. In addition, the tagging technology dropped data between 2:25pm and 2:37pm as well as between 4:07 and 5:07 pm, so any partially observed data within this time range were ignored as well. A killer whale "dive" is considered to be any continuous chunk of data that occurs below 0.5 meters in depth and lasts for at least 10 seconds. Accelerometer and depth data were smoothed by taking a moving average with a window of 1/10th of a second. Data preprocessing was done in part with the *divebomb* package in Python (Nunes, 2018). After preprocessing the raw data, a total of 267 dives were observed. Figure 6 displays the dive profile and accelerometer data.

4.2. Model Selection

The coarse-scale observations were made up of the collection of dive durations in seconds, and the fine-scale observations were determined from the within-dive acceleration data. The dive durations Y_t were assumed to follow a gamma distribution with unknown parameters $\{\mu, \sigma\}$:

$$\mathbb{E}(Y_t|X_t = i) = \mu^{(i)}$$

$$\mathbb{V}(Y_t|X_t = i) = \left(\sigma^{(i)}\right)^2$$

The acceleration exhibits significant sinusoidal behavior, so the fine-scale observations Z^* were made up of the DFT summary statistics of a two-second sliding window. Unlike the simulation study, the acceleration observations here are 3-dimensional vectors rather than scalars, so the observations z^* were calculated as follows:

$$\mathbf{z}^{*(1)}_{t,t^*} := \mathcal{R}\left(\hat{\mathbf{y}}^{*(0)}_{t,t^*}\right) \qquad z^{*(2)}_{t,t^*} := \frac{1}{100}\sum_{k=1}^{10} ||\hat{\mathbf{y}}^{(k)}_{t,t^*}||^2.$$

The observations are therefore made up of $\mathbf{z}^{*(1)}_{t,t^*}$, a 3-dimensional vector, and $z^{*(2)}_t$, a scalar. We calculate $z^{*(2)}_t$ by summing the first 10 Fourier modes, and corresponds to a maximum recorded frequency of $\tilde{\omega} = 5$ Hz. There is strong auto-correlation within $\mathbf{Z}^{*(1)}_{t,t^*}$ for all dimensions (see the supplementary material for a lag plot). Therefore, auto-correlation was directly modeled into the the distribution of $\mathbf{Z}^{*(1)}_{t,t^*}$, which is assumed to be Normally distributed with the following parameters:

$$\mathbb{E}(\mathbf{Z}^{*(1)}_{t,t^*}|\mathbf{Z}^{*(1)}_{t,t^*-1} = \mathbf{z}, X^*_{t,t^*} = i) = \phi^{*(i)}_1\mathbf{z} + (1-\phi^{*(i)}_1)\mu^{*(i)}_1$$

$$\mathbb{V}(\mathbf{Z}^{*(1)}_{t,t^*}|\mathbf{Z}^{*(1)}_{t,t^*-1} = z, X^*_{t,t^*} = i) = \text{diag}\left[\left(\sigma^{*(i)}_1\right)^2\right]$$

where $\phi^{*(i)}_1 \in \mathbb{R}$, $\mu^{*(i)}_1 \in \mathbb{R}^3$, and $\sigma^{*(i)}_1 \in \mathbb{R}^3$.

While $Z^{*(2)}_{t,t^*}$ also exhibits some auto-correlation, the relationship is less strong, and the biological interpretation of auto-correlation within $Z^{*(2)}_{t,t^*}$ is less clear. Auto-correlation was therefore not incorporated into the emission distribution of $Z^{*(2)}_{t,t^*}$. In particular, the distribution of $Z^{*(2)}_{t,t^*}$ was assumed to be gamma and parameterized by its mean and variance:

$$\mathbb{E}(Z^{*(2)}_{t,t^*}|Z^{*(1)}_{t,t^*-1} = z, X^*_{t,t^*} = i) = \mu^{*(i)}_2$$

$$\mathbb{V}(Z^{*(2)}_{t,t^*}|Z^{*(1)}_{t,t^*-1} = z, X^*_{t,t^*} = i) = \left(\sigma^{*(i)}_2\right)^2.$$

The observations $Z^{*(2)}_{t,t^*}$ and $\mathbf{Z}^{*(1)}_{t,t^*}$ were assumed to be independent of one another when conditioned of the sub-dive state X_{t,t^*}.

It is known that information criteria tends to overestimate the number of states in biological processes (Pohle et al., 2017), so we instead selected $N = 2$ dive types and $N^* = 3$ sub-dive behaviours heuristically. The absence of principled method to select the number of hidden states is a common issue in statistical ecology, so it is important to use model validation techniques in lieu of information criteria (see section 4.4).

The final model is nearly identical to the one from the simulation study, with the exception that the fine-scale Markov chain has three sub-dive behaviors instead of two ($N^* = 3$), and that the observation $\mathbf{z}^{*(1)}_{t,t^*}$ is a 3-dimensional vector rather than a scalar. The model is comprised of two levels: a coarse-scale HMM and a fine-scale CarHMM-DFT. The coarse-scale model is comprised of an HMM with hidden states corresponding to dive types and observations corresponding to dive durations. The fine-scale model is comprised of a CarHMM-DFT where auto-correlation is modeled into the distribution of $\mathbf{Z}^{*(1)}$ (the average acceleration with a 2-second window), but not $Z^{*(2)}$ (the "wiggliness" of the two second window). Refer to Figure 3 for a full graphical representation of this model.

4.3. Results

Table 2 displays estimates of the emission distribution parameters for this case study. The fitted emission distributions are also plotted in Figures 7 and 8. While the ecological meaning behind behavioral states is tenuous for HMMs, we hypothesize the following interpretations. Dive type 1 corresponds to shorter, shallower dives which serve a variety of purposes, including as rest before dives of type 2, which are deeper and more sustained. Sub-dive behavioural state 1 corresponds to gliding and less overall activity compared to the other behavioral states. The mean of $Z^{*(2)}$ in this state is at least an order of magnitude smaller than sub-dive behavioral state 2, the variance of $\mathbf{Z}^{*(1)}$ is smaller than sub-dive behavior 2 for every component, and the auto-correlation of $\mathbf{Z}^{*(1)}$ is higher than every other behavioral state. Sub-dive state 3, on the other hand, corresponds to vigorous swimming activity, as the mean of $Z^{*(2)}$ and variance of $\mathbf{Z}^{*(1)}$ for every component is much higher than every other state. The auto-correlation of $\mathbf{Z}^{*(1)}$ is also much lower in this state, implying more variation in acceleration every 2 seconds. Finally, sub-dive state 2 corresponds to a moderate amount of activity, as almost every parameter estimate is between the other two behavioral states.

The estimated probability transition matrices and associated stationary distributions are

$$\hat{\Gamma} = \begin{pmatrix} 0.849 & 0.151 \\ 0.907 & 0.093 \end{pmatrix},$$

$$\hat{\delta} = \begin{pmatrix} 0.857 & 0.143 \end{pmatrix},$$

$$\hat{\Gamma}^{*(1)} = \begin{pmatrix} 0.724 & 0.276 & 0.000 \\ 0.057 & 0.887 & 0.056 \\ 0.000 & 0.247 & 0.753 \end{pmatrix}, \qquad \hat{\Gamma}^{*(2)} = \begin{pmatrix} 0.871 & 0.129 & 0.000 \\ 0.135 & 0.829 & 0.036 \\ 0.000 & 0.246 & 0.754 \end{pmatrix},$$

$$\hat{\delta}^{*(1)} = \begin{pmatrix} 0.143 & 0.698 & 0.159 \end{pmatrix}, \qquad \hat{\delta}^{*(2)} = \begin{pmatrix} 0.476 & 0.456 & 0.067 \end{pmatrix}.$$

About 86% of observed dives are short; the whale usually rests for many dives in a row before performing a deep dive. The probability transition matrix $\hat{\Gamma}$ shows that the probability of a particular dive type does not depend much on the previous dive type. This killer whale is much more likely to be in a less active sub-dive state when performing deep dives than when performing shallow dives: sub-dive state 1 makes up 14% of shallow dives, but it makes up 48% of deep dives. Using less active sub-dive states when diving deep could be an energy reduction strategy for these long periods of holding breath. This phenomenon has been observed in bottle-nose dolphins (Williams et al., 1999) and may also be the case for killer whales. Figure 9 shows the decoded dive behavior of 5 selected dives. The supplementary material also shows the estimated *probability* of each dive time and sub-dive hidden state.

4.4. Model Validation

Two visual tools were used to evaluate this model: pseudo-residuals and empirical histograms. A pseudo-residual of a particular observation is the marginal CDF of an observation conditioned on all other observations under the learned model (Zucchini et al., 2016). To easily visualize outliers, this pseudo-residual is often passed through the quantile function of the standard Normal distribution. Mathematically, the pseudo-residual of an observation y_t in a traditional HMM is equal to $\Phi^{-1}\left(Pr(Y_t < y_t | \{Y_1, \ldots, Y_T\}/\{Y_t\})\right)$, where Φ is the cumulative distribution function of a standard Normal distribution. If the model is correct, then all pseudo-residuals are independent and follow a standard Normal distribution. We find that histograms of the pseudoresiduals of this model mostly support that the model is well-specified. $Z^{*(2)}$ is an exception, as its pseudo-residuals are noticeably right-skewed (Figure 10a). This implies that the true distribution of $Z^{*(2)}$ may follow a heavier-tailed distribution compared to a gamma distribution such as a power law.

We also plotted separate histograms of each feature where each observation was weighted by the probability that the whale was in a particular hidden state. This empirical distribution was then plotted over the fitted probability distribution function of that feature and hidden state. If the model is correct, then the histogram of each feature and hidden state should closely resemble its corresponding fitted probability distribution. See Figure 10b for an example of the dive duration. Our results mostly support a well-specified model with the exception of $Z^{*(2)}$, which is again right-skewed. In addition, $\mathbf{Z}^{*(1)}$ has heavy tails for sub-dive state 3, indicating the existence of rare events corresponding to exceptionally violent thrashing of the killer whale. These outliers are potential subjects for future study. See the supplementary material for empirical distributions of every feature and every hidden state.

5. DISCUSSION

We presented a collection of HMM models which can be combined together to form increasingly complex hierarchical models to match the complexity of particular problems faced by researchers. This flexible framework can be used to deal with complicated dependence structures within time-series data.

Traditional HMMs can be used to model a state-switching process with conditionally independent observations and Markovian dynamics when conditioned of the hidden state. However, many real-world processes are more complicated than this and require more complex models.

The CarHMM generalizes the HMM by explicitly modeling auto-correlation in the emission distributions of the HMM (Lawler et al., 2019). CarHMMs also maintain the structure needed to evaluate the likelihood using the forward algorithm. In our Normal model formulation, we have added only one additional parameter, $\phi^{(i)}$, per possible hidden state. Several useful model selection tools such as the lag plot can test if there is significant auto-correlation within an observation sequence.

Although the CarHMM can incorporate auto-correlation into the structure of an HMM, it can break down when observations are taken at irregular time intervals. A common solution to this issue is to use a continuous-time method such as the state-switching OU processes described by Michelot & Blackwell (2019). Most continuous time models require relatively slow MCMC algorithms to perform inference, and as a result are not easily incorporated into the HHMM structure. However, we show in Theorem 1 that certain continuous-time methods are equivalent to an CarHMM under certain conditions (see appendix for proof).

For simultaneous observed processes taking place at different time scales, the HHMM (Leos Barajas et al., 2017; Adam et al., 2019) utilizes hierarchical structures to jointly model both as HMMs. In particular, each hidden state of the coarse-scale HMM is assumed to emit both an observation Y_t as well as another fine-scale HMM with hidden states X_t^* and observations Y_t^*.

For processes with very high sampling frequencies and/or with intricate fine-scale structure, it is possible to generalize the HHMM such that the fine-scale model can be any model which admits an easy-to-calculate likelihood. For example, if the sampling rate of the fine-scale process is very high, then the fine-scale model can be described by a simple probability distribution over the summary statistics of a moving window of observations.

Combining these models together should be done with care, as it is important to balance the need to effectively capture the process in question with the need to avoiding over-fitting and slow parameter estimation.

One way to temper model complexity is to reduce the dimension of the parameter space by forcing fine-scale states to be shared across the coarse-scale states. Even still, model complexity inevitably grows rapidly as hierarchical structures are stacked on top of each other.

An example of balancing model complexity with efficient fitting is presented in our simulation study. Sub-dive behavioral states were shared across dive types to reduce model complexity, and by far the fastest model to train ($\approx$ 15 minutes) was the CarHMM-DFT, which had no hierarchical component. Even still, the CarHMM-DFT had near-perfect accuracy when decoding sub-dive behavioral states of the simulated whale. However, this model is not sufficient if ecologists wish to understand to joint relationship between dive type and intra-dive behaviour.

The simulation study also shows that the observed Fisher information serves as a suitable approximation for the standard errors of parameter estimates in most cases. One notable exception is that the standard errors of the probability transition matrix estimates ($\hat{\Gamma}$ and $\hat{\Gamma}^*$) tend to be overestimated by the observed Fisher information.

Finally, we used the CarHHMM-DFT to model the behavior of a killer whale off the coast of British Columbia, Canada. The CarHHMM-DFT was able to simultaneously distinguish three distinct sub-dive behaviors and two dive types. The DFT component proved useful in determining the sub-dive behaviour of the whale, as the mean of the emission distribution of $Z^{*(2)}$ for each sub-dive state was separated by an order of magnitude. Finally, the estimated auto-correlation parameter for $\mathbf{Z}^{*(1)}$, ϕ^*, was above 0.5 for every dimension and sub-dive type, providing evidence that the conditionally auto-regressive component of the CarHHMM-DFT resulted in a better fit to the data. The introduction of the parameter ϕ^* also allows $\mathbf{Z}^{*(1)}$ to be interpreted as a state-switching OU process (see appendix).

Because traditional information criteria tend to overestimate the number of states in biological processes (Pohle et al., 2017), the number of dive types and sub-dive behaviors was selected in an ad-hoc manner. There does appear to be some heterogeneity within dive types, and future work can be done to determine the optimal number of dive types and within-dive behaviors.

BIBLIOGRAPHY

T. Adam, C. Griffiths, V. Leos Barajas, E. Meese, C. Lowe, P. Blackwell, D. Righton, and R. Langrock. Joint modelling of multi-scale animal movement data using hierarchical hidden markov models. *Methods in Ecology and Evolution*, 10, 06 2019. doi: 10.1111/2041-210X.13241.

S. Bagchi and S. Mitra. *The Nonuniform Discrete Fourier Transform*. Kluwer Academic Publishing, 01 1999. doi: 10.1007/978-1-4615-1229-5_7.

G. Fehlmann, J. O'Riain, P. Hopkins, J. O'Sullivan, M. Holton, E. Shepard, and A. King. Identification of behaviours from accelerometer data in a wild social primate. *Animal Biotelemetry*, 5, 12 2017. doi: 10.1186/s40317-017-0121-3.

J. A. Green, L. G. Halsey, R. P. Wilson, and P. B. Frappell. Estimating energy expenditure of animals using the accelerometry technique: activity, inactivity and comparison with the heart-rate technique. *Journal of Experimental Biology*, 212(5):745–746, 2009. ISSN 0022-0949. doi: 10.1242/jeb.030049. URL `https://jeb.biologists.org/content/212/5/745`.

K. Heerah, M. Woillez, R. Fablet, F. Garren, S. Martin, and H. De Pontual. Coupling spectral analysis and hidden markov models for the segmentation of behavioural patterns. *Movement ecology*, 5, 09 2017. doi: 10.1186/s40462-017-0111-3.

M. Hooten, R. King, and R. Langrock. Guest editor's introduction to the special issue on "animal movement modeling". *Journal of Agricultural, Biological and Environmental Statistics*, 08 2017. doi: 10.1007/s13253-017-0299-0.

T. Jeanniard du Dot, A. Trites, J. Arnould, J. Speakman, and C. Guinet. Activity-specific metabolic rates for diving, transiting, and resting at sea can be estimated from time-activity budgets in free-ranging marine mammals. *Ecology and Evolution*, 7, 10 2016. doi: 10.1002/ece3.2546.

E. Lawler, K. Whoriskey, W. Aeberhard, C. Field, and J. Flemming. The conditionally autoregressive hidden markov model (carhmm): Inferring behavioural states from animal tracking data exhibiting conditional autocorrelation. *Journal of Agricultural, Biological and Environmental Statistics*, 05 2019. doi: 10.1007/s13253-019-00366-2.

V. Leos Barajas, E. Gangloff, T. Adam, R. Langrock, F. van Beest, J. Nabe-Nielsen, and J. Morales. Multi-scale modeling of animal movement and general behavior data using hidden markov models with hierarchical structures. *Journal of Agricultural Biological and Environmental Statistics*, 02 2017. doi: 10.1007/s13253-017-0282-9.

T. Michelot and P. Blackwell. State-switching continuous-time correlated random walks. *Methods in Ecology and Evolution*, 01 2019. doi: 10.1111/2041-210X.13154.

A. Nunes. Divebomb, 07 2018. URL `https://github.com/ocean-tracking-network/divebomb/blob/master/docs/index.rst`.

T. Patterson, A. Parton, R. Langrock, P. Blackwell, L. Thomas, and R. King. Statistical modelling of individual animal movement: an overview of key methods and a discussion of practical challenges. *AStA Advances in Statistical Analysis*, 07 2017. doi: 10.1007/s10182-017-0302-7.

J. Pohle, R. Langrock, F. van Beest, and N. Schmidt. Selecting the number of states in hidden markov models: Pragmatic solutions illustrated using animal movement. *Journal* *of Agricultural, Biological, and Environmental Statistics*, 22:1–24, 06 2017. doi: 10.1007/s13253-017-0283-8.

K. Shorter, Y. Shao, L. Ojeda, K. Barton, J. Rocho-Levine, J. Van der Hoop, and M. Moore. A day in the life of a dolphin: Using bio-logging tags for improved animal health and well-being. *Marine Mammal Science*, 06 2017. doi: 10.1111/mms.12408.

K. Whoriskey, M. Auger-Mèthè, C. Albertsen, F. Whoriskey, T. Binder, C. Krueger, and J. Flemming. A hidden markov movement model for rapidly identifying behavioral states from animal tracks. *Ecology and Evolution*, 7, 12 2016. doi: 10.1002/ece3.2795.

T. Williams, J. Haun, and W. Friedl. The diving physiology of bottlenose dolphins (tursiops truncatus): I. balancing the demands of exercise for energy conservation at depth. *The Journal of experimental biology*, 202:2739–48, 11 1999.

W. Zucchini, I. Macdonald, and R. Langrock. *Hidden Markov Models for Time Series - An Introduction Using R*. CRC Press, 06 2016. ISBN 9781482253832.

APPENDIX

Proof of Theorem 1. Combining equation (4) with equation (3) gives:

$$\left(Y_{s\Delta t} | X_{(s-1)\Delta t} = i\right) \sim \mathcal{N}\left((1-\phi^{(i)})\mu^{(i)} + \phi^{(i)} Y_{(s-1)\Delta t},\ \left(\sigma^{(i)}\right)^2\right),$$

$$s = 1, \ldots, T-1$$

If X_t follows a Markov chain with transitions at the observation times, then the behavioural state X_t does not change between observations and we can re-index $Y_{(s-1)\Delta t} = Y'_s$ and $X_{(s-2)\Delta t:(s-1)\Delta t} = X'_s$ for $s = 2, \ldots T$, yielding the desired result:

$$(Y'_s | X'_s = i) \sim \mathcal{N}\left((1-\phi^{(i)})\mu^{(i)} + \phi^{(i)} Y'_{s-1},\ \left(\sigma^{(i)}\right)^2\right)$$

$$s = 2, \ldots, T$$

X' follows a Markov chain, and the distribution of $(Y'_s | X'_s, Y'_{s+1})$ is consistent with that of a CarHMM with normal emission distributions. ■

Description of simulated data.

$\hat{Y}^*_{t,t^*}$ was simulated using the following procedure. The k^{th} Fourier mode of $\hat{Y}^*_{t,t^*}$ is denoted as $\hat{Y}^{*(k)}_{t,t^*}$:

$$
\begin{aligned}
(\hat{Y}^{*(0)}_{t,0} | X^*_{t,0} = i^*) &\sim \mathcal{N}\left(0, \sigma^{*(i^*)}\right) \\
(\hat{Y}^{*(0)}_{t,t^*} | X^*_{t,t^*} = i^*) &\sim \mathcal{N}\left(\phi^{*(i^*)} * \hat{Y}^{*(0)}_{t,t^*-1}, \sigma^{*(i^*)}\right), \quad t^* = 1, 2, \ldots, \lfloor Y_t/2 \rfloor \qquad (1) \\
\hat{Y}^{*(k)}_{t,t^*} &= a^{(k)}_{t,t^*} i \sqrt{b^{(k)}_{t,t^*}}, \qquad\qquad k = 1, \ldots, 49
\end{aligned}
$$

$$
a^{(k)}_{t,t^*} \sim \begin{cases} -1 & w.p.\ 1/2 \\ 1 & w.p.\ 1/2 \end{cases}
$$

$$
(b^{(k)}_{t,t^*} | X^*_{t,t^*} = 1) \sim \text{Gamma}(5/k^2, 1)
$$

$$
(b^{(k)}_{t,t^*} | X^*_{t,t^*} = 2) \sim \begin{cases} \text{Gamma}(5/k^2, 1), \, k \notin \{1, 2\} \\ \text{Gamma}(250, 1), & k = 1 \\ \text{Gamma}(50, 1), & k = 2 \end{cases}
$$

$$
\begin{aligned}
\hat{Y}^{*(50)}_{t,t^*} &= 0 \\
\hat{Y}^{*(k)}_{t,t^*} &= -\hat{Y}^{*(100-k)}_{t,t^*}, \qquad\qquad k = 51, \ldots, 99
\end{aligned}
$$

$Y^*_{t,t^*,1:100}$ was set using the inverse discrete Fourier transform of $\hat{Y}^*_{t,t^*}$:

$$
Y^*_{t,t^*,1:100} = IDFT\left(\hat{Y}^*_{t,t^*}\right), \qquad t^* = 1, \ldots, \lfloor Y_t/2 \rfloor
$$

$\hat{Y}^{*}_{t,t^*}$ is anti-symmetric about $\hat{Y}^{*(50)}_{t,t^*}$ so that its inverse Fourier transform is real-valued. $\hat{Y}^{*(k)}_{t,t^*}$ also decays like $1/k$ so that Y^{*}_{t,t^*} remains continuous within a two-second window. Y^{*}_{t,t^*} is not continuous *between* windows, but the jump discontinuities are not very severe since $\hat{Y}^{*(0)}_{t,t^*}$ and $\hat{Y}^{*(0)}_{t,t^*+1}$ are highly correlated. See Figure 2 for details.

From here it is straightforward to calculate both $Z^{*(1)}$ and $Z^{*(2)}$. We pick $\tilde{\omega} = 10$ periods per window, or 5 hertz. To find the distribution of $Z^{*(1)}_{t,t^*} = \mathcal{R}\left(\hat{Y}^{(0)}_{t,t^*}\right)$, use Equation (1):

$$\left(Z^{*(1)}_{t,t^*} | X^{*}_{t,t^*} = i^*\right) = \left(\mathcal{R}\left(\hat{Y}^{(0)}_{t,t^*}\right) | X^{*}_{t,t^*} = i^*\right) \sim \mathcal{N}\left(\phi^{*(i^*)} * Z^{*(1)}_{t,t^*-1}, \sigma^{*(i^*)}\right)$$

$Z^{*(2)}_{t,t^*}$ is the sum of gamma-distributed random variables with the same scale parameter, so the distribution of $Z^{*(2)}_{t,t^*}$ is also a gamma distribution:

$$Z^{*(2)}_{t,t^*} = \sum_{k=1}^{10} b^{(k)}_{t,t^*}$$

$$\left(Z^{*(2)}_{t,t^*} | X^{*}_{t,t^*} = 1\right) \sim \text{Gamma}\left(\alpha = \sum_{k=1}^{10} 5/k^2 = 10.10, \beta = 1.00\right)$$

$$\left(Z^{*(2)}_{t,t^*} | X^{*}_{t,t^*} = 1\right) \sim \text{Gamma}\left(\alpha = 300 + \sum_{k=3}^{10} 5/k^2 = 305.94, \beta = 1.00\right)$$

■

Likelihood of Simulation study model.

The overall likelihood of the CarHHMM-DFT model is as follows:

$$\mathcal{L}_{\text{CarHHMM-DFT}}(y, z^*; \Theta, \Theta^*, \Gamma, \Gamma^*) = \delta P(y_1, z_1^*; \Theta, \Theta^*, \Gamma^*) \prod_{t=2}^{T} \Gamma P(y_t, z_t^*; \Theta, \Theta^*, \Gamma^*) \mathbf{1}_N$$

where:

$$P(y_t, z_t^*; \Theta, \Theta^*, \Gamma^*) = \text{diag}\Big[f^{(1)}(y_t; \Theta^{(i)}) \mathcal{L}_{\text{CarHMM-DFT}}\left(z_t^*; \Theta^{*(1)}, \Gamma^{*(1)}\right), \ldots, \\ f^{(N)}(y_t; \Theta^{(i)}) \mathcal{L}_{\text{CarHMM-DFT}}\left(z_t^*; \Theta^{*(N)}, \Gamma^{*(N)}\right) \Big]$$

$f^{(i)}(y_t; \Theta^{(i)})$ is the emission distribution of the dive duration y_t conditioned on the fact that $X_t = i$.

$\mathcal{L}_{\text{CarHMM-DFT}}$ corresponds to the fine-scale chain:

$$\mathcal{L}_{\text{CarHMM-DFT}}\left(z_t^*; \Theta^{*(i)}, \Gamma^{*(i)}\right) = \delta^{*(i)} \prod_{t=2}^{T} \Gamma^{*(i)} P(z_{t,t^*}^* | z_{t,t^*-1}^*; \Theta^{*(i^*)}) \mathbf{1}_N$$

where $P(z_{t,t^*}^* | z_{t,t^*-1}^*; \Theta^{*(i)})$ is an $N^* \times N^*$ diagonal matrix with $(i^*, i^*)^{th}$ entry equal to $f^{(i,i^*)}(z_{t,t^*}^* | z_{t,t^*-1}^*; \theta^{*(i,i^*)})$. $f^{(i,i^*)}(z_{t,t^*}^* | z_{t,t^*-1}^*; \theta^{*(i,i^*)})$ is the emission distribution of Z_{t,t^*}^* conditioned on $X_{t,t^*}^* = i^*$ and $Z_{t,t^*-1}^* = z_{t,t^*-1}^*$.

■

1. FIGURES AND TABLES

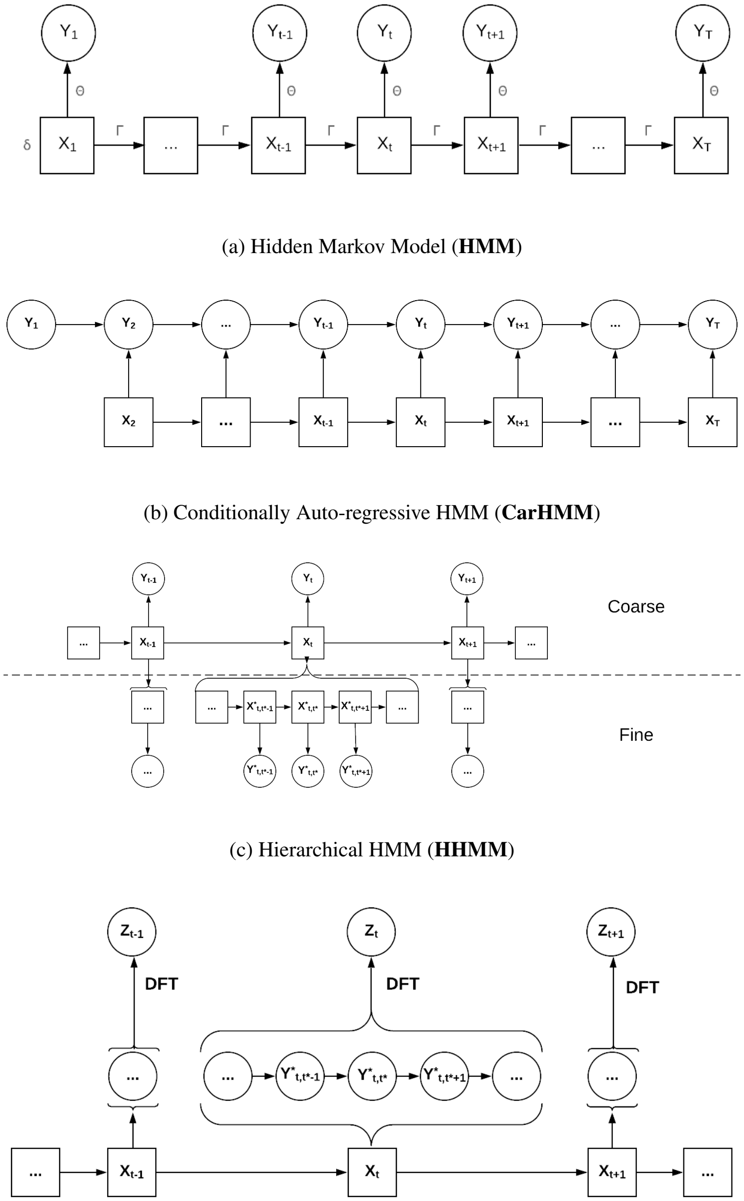

(a) Hidden Markov Model (**HMM**)

(b) Conditionally Auto-regressive HMM (**CarHMM**)

(c) Hierarchical HMM (**HHMM**)

(d) HMM with Discrete Fourier Transform (**HMM-DFT**)

FIGURE 1: : Graphical representations of HMM models

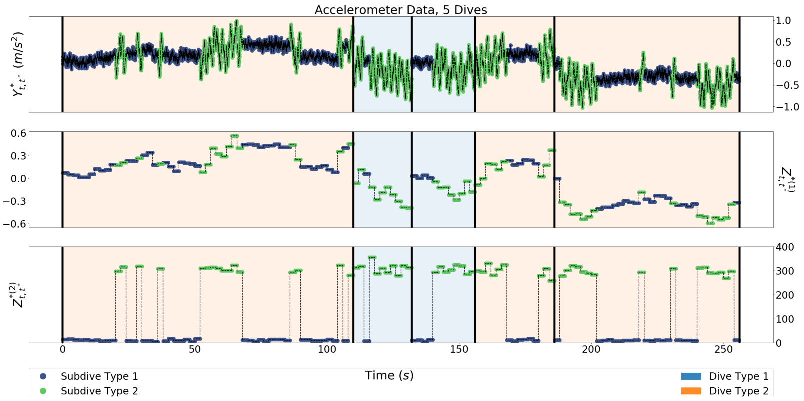

FIGURE 2: : Simulated acceleration data for one dive. The color of the line corresponds to the true fine-scale state of the sub-dive process, while the color of the background corresponds to the true dive type of the simulated whale.

TABLE 1: : Accuracies and run times for all models. All reported values are averages, and ± refers to the standard deviation.

Model	Training Time (Minutes)	Dive Accuracy	Subdive Accuracy
CarHMM-DFT	15.74 ± 2.46	———–	1.00 ± 0.00
HHMM-DFT	82.43 ± 11.48	0.94 ± 0.02	1.00 ± 0.00
CarHHMM	70.85 ± 15.89	0.91 ± 0.03	0.89 ± 0.02
CarHHMM-DFT	81.22 ± 16.10	0.94 ± 0.02	1.00 ± 0.00

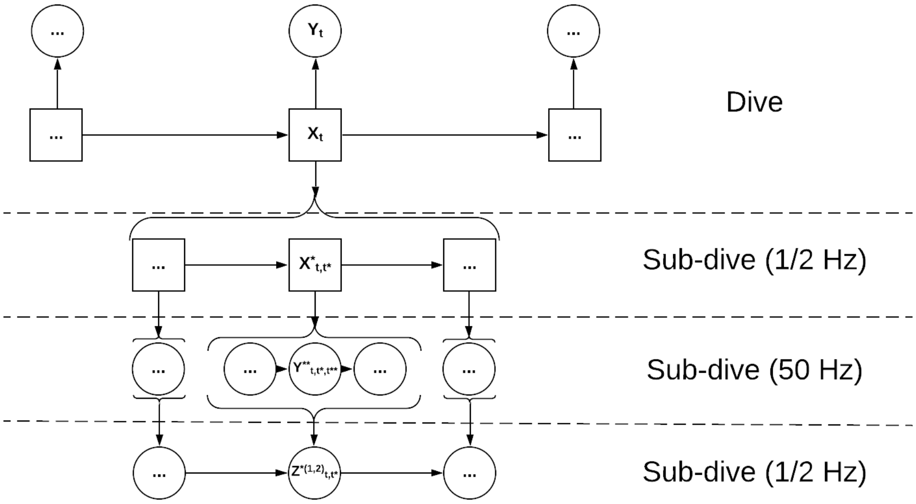

FIGURE 3: : Graphical representation the model used in the simulation and case study, the **CarHHMM-DFT**.

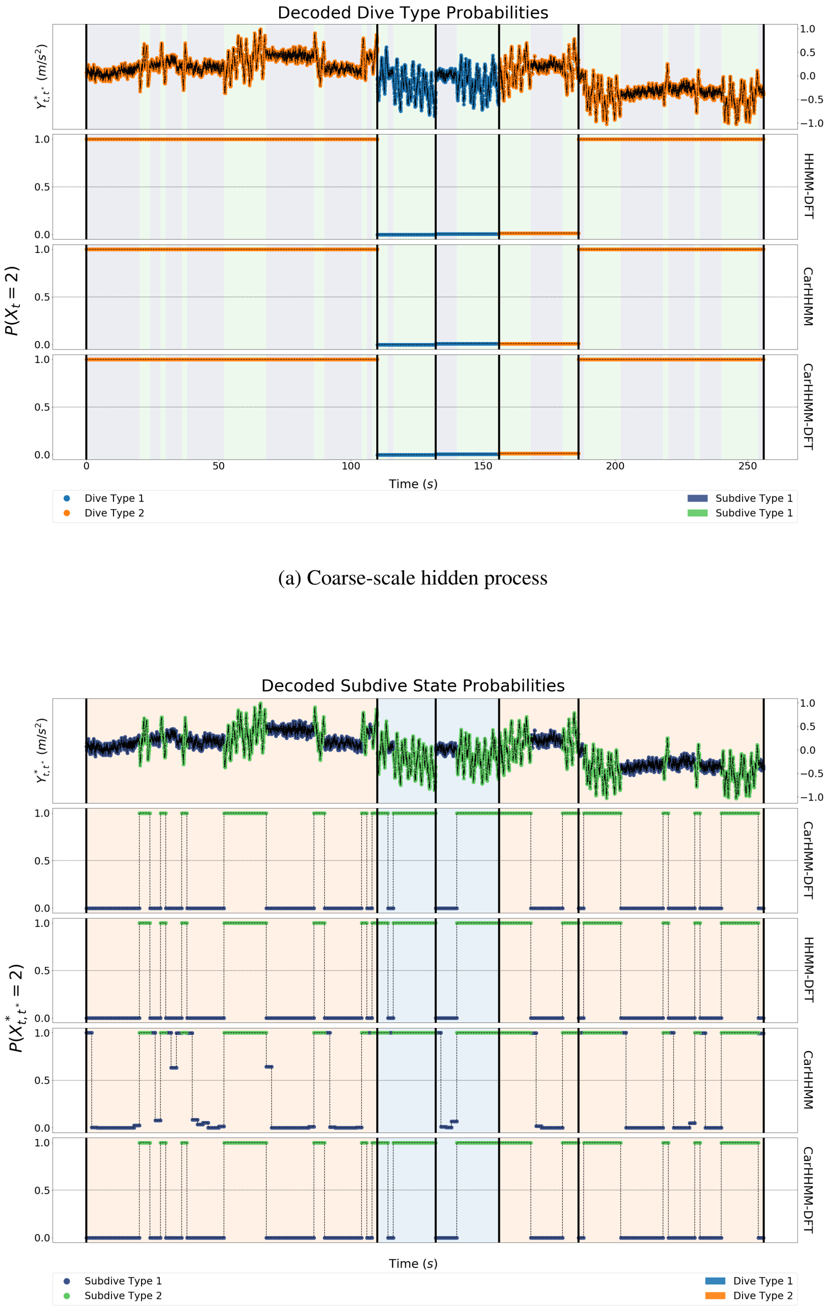

(a) Coarse-scale hidden process

(b) Fine-scale hidden process

FIGURE 4: : Decoded state probabilities of each model

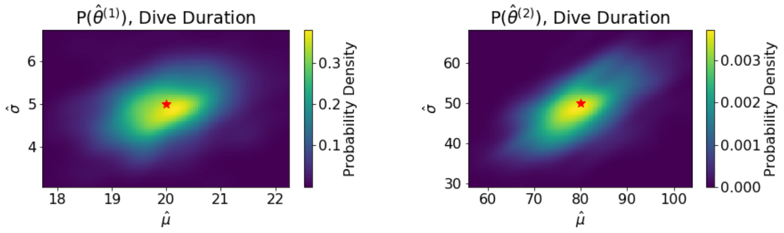

(a) Dive Type 1

(b) Dive Type 2

FIGURE 5: : KDE plot of $\hat{\mu}$ and $\hat{\sigma}$ for the dive duration emission distribution for the CarHMM.

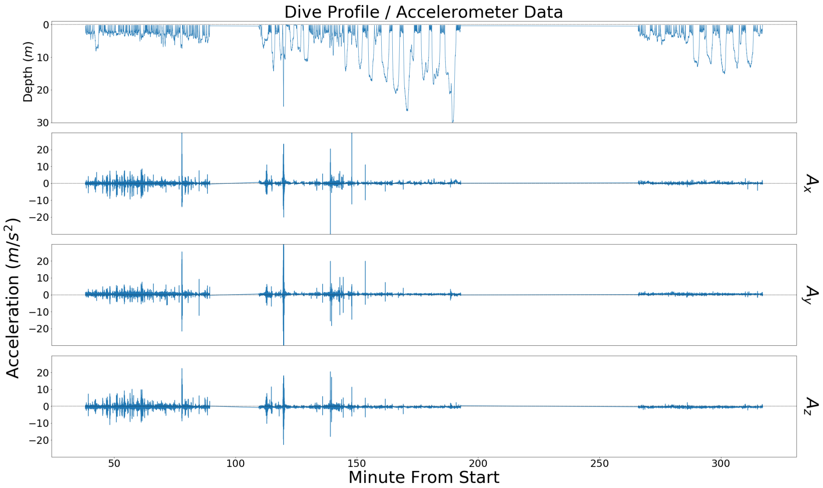

FIGURE 6: : Dive profile and Accelerometer data of killer whale data set

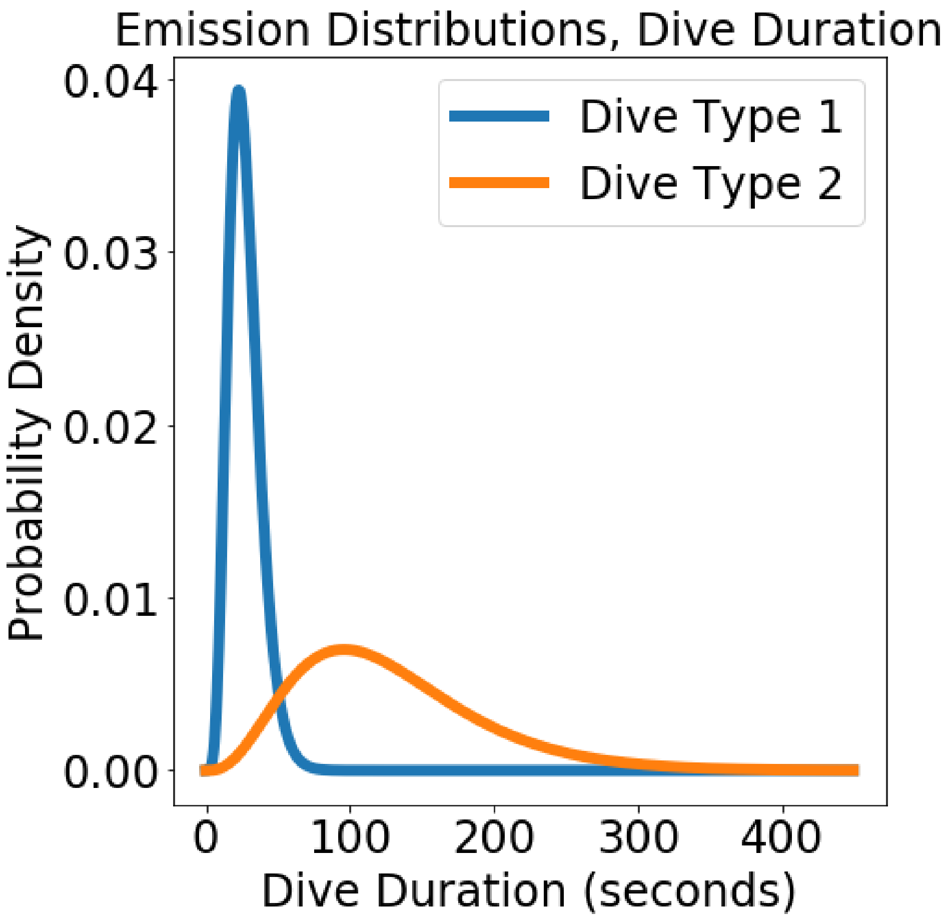

FIGURE 7: : Estimated probability distributions for each coarse-scale observation in each dive type.

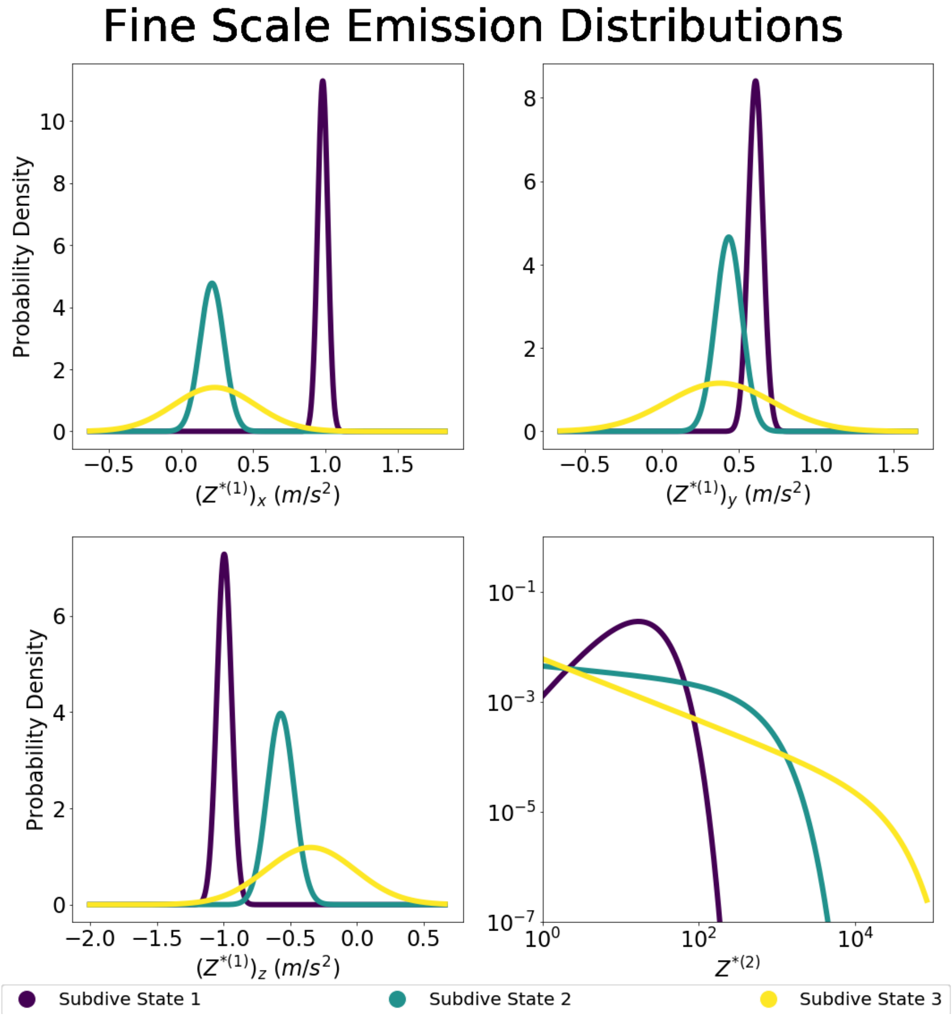

FIGURE 8: : Estimated probability distributions for each fine-scale observation in each behavioral state. Note that the distributions of acceleration do not take auto-correlation into account (see table 2)

TABLE 2: : Estimates and standard errors of emission parameters for killer whale data.

Feature	Dive / Sub-dive Type	Parameter Estimate		
		$\hat{\mu}$	$\hat{\sigma}$	$\hat{\phi}$
Dive Duration (s) - Y	1	27.23 ± 0.63	10.89 ± 0.56	—
	2	127.96 ± 11.50	64.13 ± 9.21	—
x-acceleration (m/s^2) - $\left(\mathbf{Z}^{*(1)}\right)_x$	1	0.98 ± 0.07	0.04 ± 0.00	0.99 ± 0.00
	2	0.22 ± 0.01	0.08 ± 0.00	0.87 ± 0.01
	3	0.23 ± 0.03	0.28 ± 0.01	0.62 ± 0.03
y-acceleration (m/s^2) - $\left(\mathbf{Z}^{*(1)}\right)_y$	1	0.61 ± 0.09	0.05 ± 0.00	0.99 ± 0.00
	2	0.43 ± 0.01	0.09 ± 0.00	0.87 ± 0.01
	3	0.38 ± 0.04	0.35 ± 0.01	0.62 ± 0.04
z-acceleration (m/s^2) - $\left(\mathbf{Z}^{*(1)}\right)_z$	1	-1.00 ± 0.11	0.05 ± 0.00	0.99 ± 0.00
	2	-0.57 ± 0.01	0.10 ± 0.00	0.87 ± 0.01
	3	-0.35 ± 0.04	0.34 ± 0.01	0.62 ± 0.04
Fourier sum - $Z^{*(2)}$	1	27.16 ± 0.32	16.67 ± 0.32	—
	2	406.98 ± 4.42	438.09 ± 5.49	—
	3	9688.54 ± 221.95	14584.02 ± 358.40	—

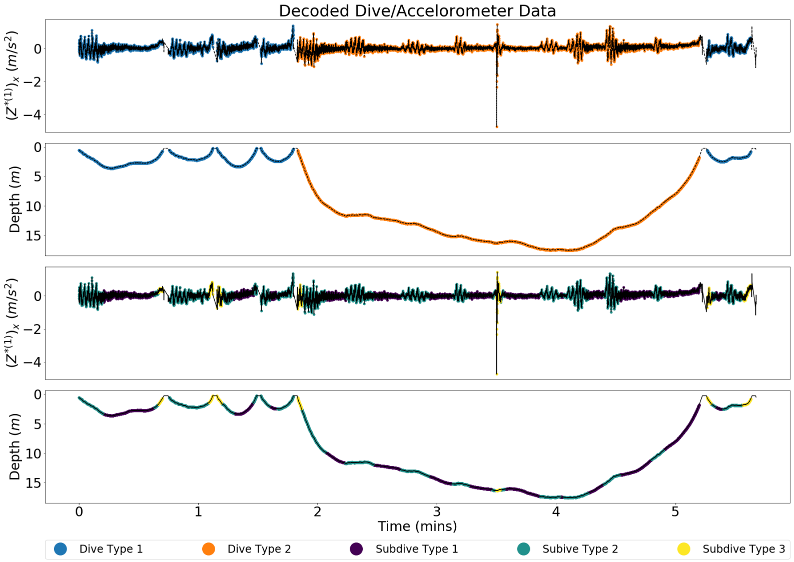

FIGURE 9: : Features of a particular set of killer whale dives and decoded estimates for the intra-dive behavioral states. The color of the plot corresponds to behavioral or dive state with the highest probability.

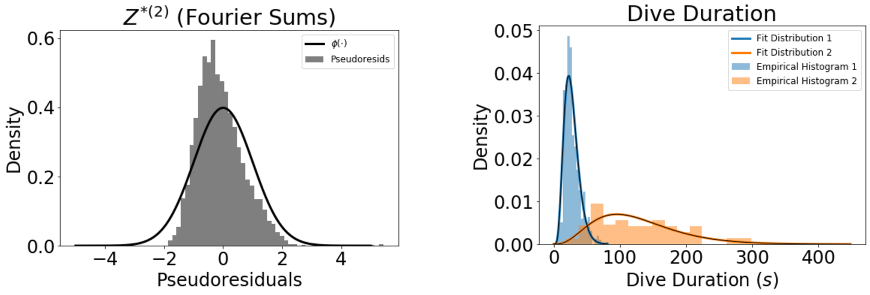

(a) Pseudoresiduals of $Z^{*(2)}$

(b) Empirical distribution of Y (Dive Duration)

FIGURE 10: : Examples of psuedoresiduals and a weighted empirical distribution as a model checking tool.